

Unveiling Eigenstate Thermalization for Non-Hermitian systems

Sudipto Singha Roy,^{1,2,*} Soumik Bandyopadhyay,^{1,2,*} Ricardo Costa de Almeida,^{1,2} and Philipp Hauke^{1,2,†}

¹*Pitaevskii BEC Center, CNR-INO and Dipartimento di Fisica,
Universit'a di Trento, Via Sommarive 14, Trento, I-38123, Italy*

²*INFN-TIFPA, Trento Institute for Fundamental Physics and Applications, Trento, Italy*

(Dated: September 4, 2023)

The Eigenstate Thermalization Hypothesis (ETH) has been highly influential in explaining thermodynamic behavior of closed quantum systems. As of yet, it is unclear whether and how the ETH applies to non-Hermitian systems. Here, we introduce a framework that extends the ETH to non-Hermitian systems. It hinges on a suitable choice of basis composed of right eigenvectors of the non-Hermitian model, a choice we motivate based on physical arguments. In this basis, and after correctly accounting for the nonorthogonality of non-Hermitian eigenvectors, expectation values of local operators reproduce the well-known ETH prediction for Hermitian systems. We illustrate the validity of the modified framework on non-Hermitian random-matrix and Sachdev–Ye–Kitaev models. Our results thus generalize the ETH to the non-Hermitian setting, and they illustrate the importance of the correct choice of basis to evaluate physical properties.

Introduction.— The Eigenstate Thermalization Hypothesis (ETH) [1–7] plays an instrumental role in understanding the thermalization of closed quantum systems. Its central claim is that expectation values of generic local observables of non-integrable models follow a simple form that depends only on smooth functions of energy and density of states. Over the past years, tremendous efforts have been put into understanding the applicability of the ETH, for a wide variety of models [8–34]. However, with the exception of Ref. [35], none of these cover models described by non-Hermitian Hamiltonians. Non-Hermitian systems show a large variety of intriguing phenomena not present in their Hermitian counterparts, including complex eigenspectra [36–41], exceptional points [40, 42–45], coalescence of eigenstates [46, 47], the non-Hermitian skin effect [48–50], and non-Hermitian linear response [51, 52], and they have been proposed as platforms for quantum-enhanced sensing [53–58]. The widespread theoretical effort for achieving a deeper understanding is going hand in hand with a strong advance in the experimental control over non-Hermitian systems [45, 47, 59–63]. Despite their rising importance, it remains an outstanding challenge to understand the emergence of ETH in the context of non-Hermitian systems.

In this letter, we establish a framework for the ETH in non-Hermitian systems. Specifically, we construct a modified ansatz that enables us to generalize the celebrated Hermitian ETH ansatz. It accounts for the non-orthogonality of eigenstates of non-Hermitian Hamiltonians, and enables us to correctly describe both diagonal and off-diagonal matrix elements of local expectation values. The framework hinges on a suitable choice of basis, composed of right eigenvectors. We motivate this basis choice on physical grounds, as it defines well-behaved

quantum states that can be naturally prepared through non-Hermitian evolution (see Fig. 1). By contrast, the recent work of Ref. [35] chose a biorthogonal basis, leading to expectation values incompatible with ETH predictions. We confirm our framework through detailed numerics on non-Hermitian random matrix ensembles as well as non-Hermitian versions of the Sachdev–Ye–Kitaev (SYK) model. Our work thus unveils how the ETH extends to non-Hermitian systems, and it illustrates the importance of an appropriate choice of basis for the evaluation of physical behavior in non-Hermitian systems, with consequences reaching beyond the immediate context.

In what follows, we first give some background on the Hermitian ETH and the findings of Ref. [35]. We then present our arguments onto why the basis of right eigenvectors should be used. From that, we derive our main formalism, first focusing on the non-Hermitian random Ginibre ensemble [64–68] and then on the non-Hermitian SYK model [34, 69–72]. The conclusions put the findings into broader context.

Background.— Though not proven, the ETH has been widely tested in Hermitian systems. Its central claim is that the expectation value of a generic local observable \hat{O} , when computed in the energy eigenbasis of a non-integrable model, given by basis states $\{|m\rangle\}$, follows a surprisingly simple and general form [6]:

$$O_{mn} = \langle m | \hat{O} | n \rangle = O(\bar{E}) \delta_{mn} + e^{-S(\bar{E})/2} f(\bar{E}, \omega) d_{mn}. \quad (1)$$

Here, $\bar{E} = \frac{E_m + E_n}{2}$ is the mean energy of the considered eigenstates, $\omega = |E_m - E_n|$ their absolute energy difference, $S(\bar{E})$ is the entropy, and d_{mn} 's are Gaussian random numbers (real or complex) with zero mean and unit variance (see also [73–76]). Important and non-trivial features are the smoothness of $O(\bar{E})$ and $f(\bar{E}, \omega)$, as well as the strong decrease in fluctuations with density of states (entering through the entropy). As a result, differ-

* These two authors contributed equally

† philipp.hauke@unitn.it

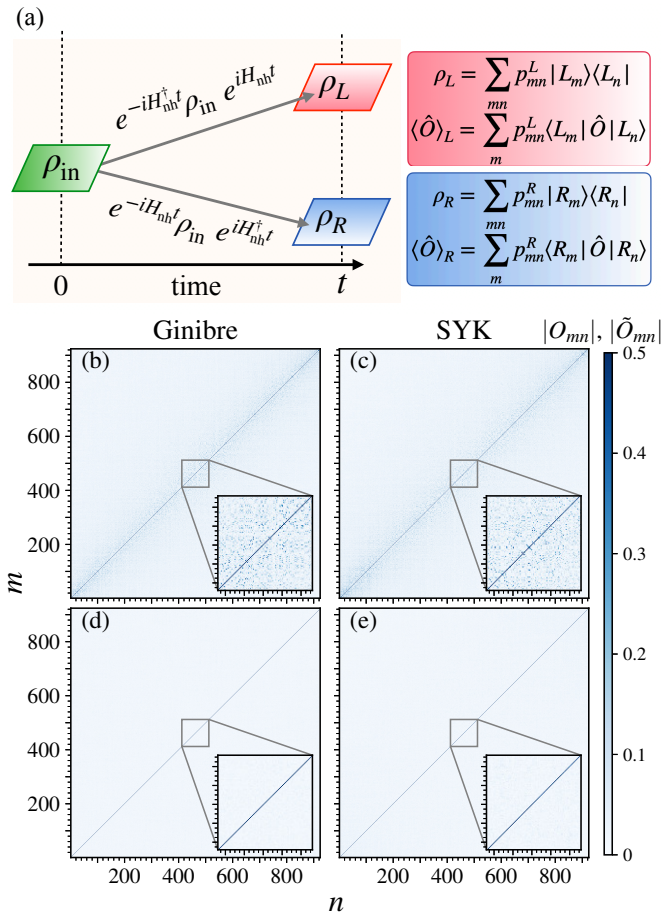


Figure 1. (a) The evolution under a generic non-Hermitian Hamiltonian H_{nh} (H_{nh}^\dagger) naturally leads to measuring the expectation value of an operator \hat{O} in right (left) eigenvectors only. (b,c) $|\langle R_m | \hat{O} | L_n \rangle|$ for a non-Hermitian random matrix (b) and SYK model (c), for a single realization and system size $N = 12$. Unlike the behavior obtained for the biorthogonal basis (see Appendix D), diagonal elements ($m = n$) show the signatures of ETH. However, the bare off-diagonal elements ($m \neq n$) exhibit significant non-zero contributions (see zooms). (d,e) Once we correct for the off-diagonal contribution that comes solely from the nonorthogonality of eigenvectors (see Eq. (10)), the behavior is similar to the Hermitian counterpart and in agreement with ETH.

ent states with a given energy E are—for what concerns local observables—indistinguishable from each other, as well as from a microcanonical ensemble at the same energy density.

The above relation also provides a connection to the behavior of observables according to random matrix theory (RMT) [6], which specializes Eq. (1) to

$$O_{mn} = \langle m | \hat{O} | n \rangle = \bar{O} \delta_{mn} + \tilde{d}_{mn} \sqrt{\frac{\overline{O^2}}{\mathcal{D}}}, \quad (2)$$

where \bar{O} is the mean of the observable, \mathcal{D} is the Hilbert space dimension, and \tilde{d}_{mn} is a random variable similar

to d_{mn} .

It is *a priori* not obvious how to apply these relations to non-Hermitian systems. In particular, one unusual property of non-Hermitian Hamiltonians is that their left and right eigenvectors are orthogonal but not necessarily the Hermitian conjugate of each other. In formulas, a non-Hermitian Hamiltonian can be diagonalized as

$$H_{\text{nh}} = \sum_m \varepsilon_m |R_m \rangle \langle L_m|, \quad (3)$$

with $\langle L_m | R_n \rangle = \delta_{mn}$ but $\langle L_m | \neq (|R_m \rangle)^\dagger$ is possible. This behavior of H_{nh} has led to diverging attempts when trying to analyze its properties: it is currently unclear whether one should choose the state of interest as $\rho_m^{RR} = |R_m \rangle \langle R_m|$, as $\rho_m^{LL} = |L_m \rangle \langle L_m|$, or, using the biorthogonal basis states, as $\rho_m^{RL} = |R_m \rangle \langle L_m|$ [77, 78]. In particular, when defining the “ground state” of H_{nh} as $\rho_0^{RL} = |R_0 \rangle \langle L_0|$, results such as complex entanglement entropy appear [78, 79], which lack clear physical interpretation.

In Ref. [35], it was argued that the non-Hermitian version of the SYK model fails to satisfy the ETH as given by Eq. (1). Namely, expectation values of a local operator \hat{O} computed in the biorthogonal basis, i.e., $|\langle R_m | \hat{O} | L_n \rangle|$, show fluctuations for both on and off diagonal matrix elements that are comparable to the mean. The numerical claims have been supported by analytical predictions obtained using the non-Hermitian RMT comprising the Ginibre [64] and other ensembles. In what follows, we (i) provide arguments why the right eigenvectors are physically preferred to evaluate matrix elements, $|\langle R_m | \hat{O} | R_n \rangle|$, and (ii) show that on this basis ETH is fulfilled under a straightforward modification.

Preferability of right eigenbasis.—To a considerable part, the significance of the ETH for Hermitian systems stems from its relevance to time evolution of closed quantum systems. For a non-Hermitian Hamiltonian H_{nh} , an initial state ρ_{in} evolves into

$$\begin{aligned} \rho(t) &= e^{-itH_{\text{nh}}} \rho_{\text{in}} e^{itH_{\text{nh}}^\dagger}, \\ &= \sum_{mn} e^{-it\phi_{mn}} a_{mn} |R_m \rangle \langle R_n|. \end{aligned} \quad (4)$$

Here, $a_{mn} = \langle L_m | \rho_{\text{in}} | L_n \rangle$ and $\phi_{mn} = \varepsilon_m - \varepsilon_n^*$.

As this equation shows, expectation values of observables, $\text{Tr}(\rho(t)\hat{O})$, will be determined by the matrix overlap elements $\langle R_n | \hat{O} | R_m \rangle$ (see schematic in Fig. 1(a), and Appendix A for details and specific cases). The relevance of the right eigenvectors to time-evolution of non-Hermitian systems has also been noted, e.g., in Ref. [80]. The left eigenvectors appear in the above expression only through the overlap with the initial state, via a_{mn} . The roles of $|R_m \rangle$ and $|L_m \rangle$ can be inverted by considering the time evolution generated by H_{nh}^\dagger instead of H_{nh} , but mixed matrix elements of the form $\langle R_n | \hat{O} | L_m \rangle$ do not

naturally appear. Motivated by the above operational interpretation, below we will use the basis given by the right eigenvectors.

Formalism and non-Hermitian RMT analysis.—The formalism we introduce here is best illustrated through a non-Hermitian RMT analysis. Statistical properties of typical chaotic non-Hermitian systems can be modeled by drawing the elements of H_{nh} from the complex Ginibre ensemble [65–68] (see Appendix B for details). As a local observable of interest, we choose one that is similar to what we will use to probe the non-Hermitian SYK model below. Specifically, we choose the single-mode number operator $\hat{O} = \hat{n}_i = c_i^\dagger c_i$, where c_i^\dagger (c_i) is the creation (annihilation) operator for the i th fermionic mode. Additionally, as we will restrict our studies of the SYK model to the half-filling sector, we choose H_{nh} as a $\mathcal{D} \times \mathcal{D}$ random matrix with $\mathcal{D} = {}^N C_{N/2}$. Moreover, throughout this work, we consider the right eigenvectors to be properly normalized, i.e., $\langle R_m | R_m \rangle = 1$. We now provide a systematic analysis of both diagonal and off-diagonal terms of $\langle R_m | \hat{O} | R_n \rangle$.

Diagonal terms: Figure 1(b) illustrates the overall behavior of $O_{mn} = |\langle R_m | \hat{O} | R_n \rangle|$ for $N = 12$ and one single instance of random realization. For a more quantitative analysis, Fig. 2(a) reports the diagonal terms ($m = n$) for different system sizes $N = 8, 10, 12, 14, 16$ against $|\epsilon_m|$. As this data shows, fluctuations around the mean $\bar{O} = \frac{1}{\mathcal{D}} \sum_p \langle p | \hat{O} | p \rangle$ are strongly suppressed with system size. Here, $|p\rangle = |p_1, \dots, p_N\rangle$ are the basis states of the fermionic Fock space. Two insets provide further quantitative support: In the bottom left inset of Fig. 2(a), we plot the histogram of $[O_{mm} - \bar{O}]$ obtained using all the eigenstates lying within the energy disk of radius $|\epsilon_m| = 0.2$ (indicated in the top inset), for 20 random realizations of the model and $N = 16$ (see also Appendix C). The data is well-fitted by a Gaussian profile (black dashed line). Moreover, in the right inset we display the variance of $[O_{mm} - \bar{O}]$, $\langle \langle \sigma_d^2 \rangle \rangle$, against Hilbert space dimension \mathcal{D} , exhibiting a clear exponential decay with system size, a property also found in non-integrable Hermitian systems [10, 73, 75].

This behavior remains thus close to the RMT prediction for Hermitian systems, i.e., for a single instance of random realization we find

$$O_{mm} = \langle R_m | \hat{O} | R_m \rangle = \bar{O} + Q_{mm} \sqrt{\frac{\bar{O}^2}{\mathcal{D}}}, \quad (5)$$

where the second term describes the exponentially decreasing fluctuations of $\langle R_m | \hat{O} | R_m \rangle$ governed by independent random numbers Q_{mm} .

Off-diagonal terms: As Fig. 1(b) illustrates, the off-diagonal elements $|\langle R_m | \hat{O} | R_n \rangle|_{m \neq n}$ have significantly less structure than the elements evaluated in the biorthogonal basis (see Appendix D). At first sight, this result is nevertheless still not compatible with ETH, as

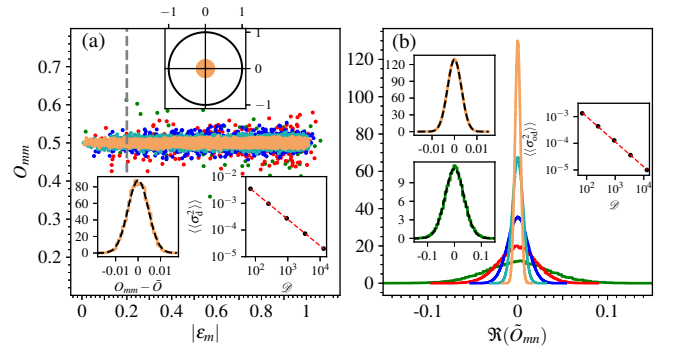


Figure 2. Signature of ETH in a random non-Hermitian Hamiltonian from the Ginibre ensemble. (a) Diagonal elements of the local observable \hat{O} computed in the right eigenvectors, $|O_{mm}| = |\langle R_m | \hat{O} | R_m \rangle|$, against $|\epsilon_m|$, for system sizes $N = 8, 10, 12, 14, 16$ (green, red, blue, sea green, orange) and a single random realization. With increasing size, fluctuations are suppressed and O_{mm} tend to converge to $\bar{O} = 0.5$. Bottom left inset: Histogram of $[O_{mm} - \bar{O}]$ for eigenstates within $|\epsilon_m| \leq 0.2$ (top inset), for $N = 16$ and for 20 random realizations. The profile is fitted well with a Gaussian distribution (black dashed). Bottom right inset: Fluctuations, as measured by the variance $\langle \langle \sigma_d^2 \rangle \rangle$ of $[O_{mm} - \bar{O}]$, shows a perfect linear decay (having slope ≈ 0.99) with the Hilbert space dimension \mathcal{D} in logarithmic scale, thus confirming an exponential decrease with system size (data for 5000, 1000, 500, 200, and 20 realizations from $N = 8$ to $N = 16$). (b) Histogram of the real part of the off-diagonal terms $\tilde{O}_{mn} = O_{mn} - \langle R_m | R_n \rangle \bar{O}$, $m \neq n$, again obtained for energy states with $|\epsilon_m| \leq 0.2$ but for different system sizes, $N = 8, 10, 12, 14, 16$ (green, red, blue, sea green, orange), with 5000, 1000, 500, 200, 20 random realizations, respectively. The profiles can be accurately fitted by a Gaussian distribution, as exemplified for $N = 8$ (left top inset) and $N = 16$ (left bottom inset). As for the diagonal case, the variance of the off-diagonal terms \tilde{O}_{mn} , $\langle \langle \sigma_{\text{od}}^2 \rangle \rangle$, also exhibits exponential decay with system size (right inset). In this case the fitted slope ≈ 0.94 .

the inset of Fig. 1(b) shows, since (i) there is some remaining structure and (ii) the off-diagonal terms do not get suppressed with Hilbert space dimension even at moderately large system size. The reason lies in the unusual orthogonality relations of non-Hermitian eigenstates. In what follows, we first detail the physical reasoning, based on which we then present the necessary modification of Eq. (1) that restores the notion of ETH for the off-diagonal terms.

As mentioned before, the right eigenvectors of a non-Hermitian system can be nonorthogonal, $\langle R_m | R_n \rangle \neq 0$ for $m \neq n$. However, one can always isolate the (normalized) component of $|R_n\rangle$ orthogonal to $|R_m\rangle$, $|R_{n\perp m}\rangle$, through the decomposition

$$|R_n\rangle = \alpha_{nm} |R_m\rangle + \beta_{nm} |R_{n\perp m}\rangle, \quad (6)$$

where $\alpha_{nm} = \langle R_m | R_n \rangle$ and $\beta_{nm} = \langle R_{n\perp m} | R_n \rangle$. Using this relation, we get

$$\langle R_m | \hat{O} | R_n \rangle_{m \neq n} = \alpha_{nm} O_{mm} + \beta_{nm} \langle R_m | \hat{O} | R_{n\perp m} \rangle. \quad (7)$$

Since $|R_m\rangle$ and $|R_{n\perp m}\rangle$ are orthonormal random vectors, we can expect the second term to behave as per the prediction from the Hermitian ETH, Eq. (2), i.e., to be of the form $\beta_{nm}\tilde{Q}_{mn}\sqrt{\frac{O^2}{\mathcal{D}}}$, with \tilde{Q}_{mn} a random number. Using the ETH for the diagonal elements as established above, the first term will behave as $\alpha_{nm}\bar{O} + \alpha_{nm}Q_{mm}\sqrt{\frac{O^2}{\mathcal{D}}}$. The randomly fluctuating parts can be collected into a term $S_{mn}\sqrt{\frac{O^2}{\mathcal{D}}}$, where $S_{mn} = \alpha_{nm}Q_{mm} + \beta_{nm}\tilde{Q}_{mn}$ is again a random number. This term would obey the ETH for off-diagonal elements, as prescribed for the Hermitian ETH, Eq. (2). There remains, however, a further contribution to the off-diagonal elements that derives from the non-orthogonality of eigenvectors, $\alpha_{nm}\bar{O}$. As generically in non-Hermitian systems $\alpha_{nm} = \langle R_m|R_n\rangle \neq 0$, even at moderately large system size $\langle R_m|\hat{O}|R_n\rangle$ can thus still have a significant nonzero value. We hence need to suitably modify the ETH relation.

Summarizing the above considerations, we can thus conjecture the generalized version of the ETH ansatz for a non-Hermitian random matrix: *The matrix elements of any local observable, \hat{O} , obeying the ETH ansatz for any generic normalized basis $\{|R_m\rangle\}$ of a non-Hermitian random matrix Hamiltonian should behave as*

$$O_{mm} = \langle R_m|\hat{O}|R_m\rangle = \bar{O} + Q_{mm}\sqrt{\frac{O^2}{\mathcal{D}}}, \quad (8)$$

$$O_{mn} = \langle R_m|\hat{O}|R_n\rangle_{m\neq n} = \langle R_m|R_n\rangle\bar{O} + S_{mn}\sqrt{\frac{O^2}{\mathcal{D}}}. \quad (9)$$

In case of Hermitian systems, $\langle R_m|R_n\rangle = \delta_{mn}$ and we recover the familiar prediction of Eq. (2) as a special case. In analogy with Eq. (1), we can also conjecture that for a generic non-Hermitian system, \bar{O} and $\sqrt{\frac{O^2}{\mathcal{D}}}$ should be replaced by smooth functions of the (complex) average energy \bar{E} and energy difference ω .

We present the numerical results supporting Eqs. (8, 9) in Fig. 1(d), where we plot the absolute value of

$$\tilde{O}_{mn} = \begin{cases} O_{mn} & \text{for } m = n, \\ O_{mn} - \langle R_m|R_n\rangle\bar{O} & \text{for } m \neq n. \end{cases} \quad (10)$$

As the figure illustrates, the modification of the off-diagonal terms unveils a behavior of the local observable exactly analogous to the prediction for the Hermitian systems. Moreover, as the histograms of $\Re[\tilde{O}_{mn}]_{n\neq m}$, plotted in Fig. 2(b), show, \tilde{O}_{mn} gets suppressed with increasing system size and approximates a Gaussian profile. Additionally, analogously to the Hermitian case [6, 81], the ratio of the variance of diagonal (O_{mm}) and modified off-diagonal (\tilde{O}_{mn}) expectation values becomes $\frac{\langle\langle\sigma_d^2\rangle\rangle}{\langle\langle\sigma_{od}^2\rangle\rangle} \approx 2$. All these observations strongly corroborate the signature of ETH in the non-Hermitian random Hamiltonian H_{nh} .

Sachdev-Ye-Kitaev model.—In the final part of our work, we confirm the prediction given in Eqs. (8, 9) for

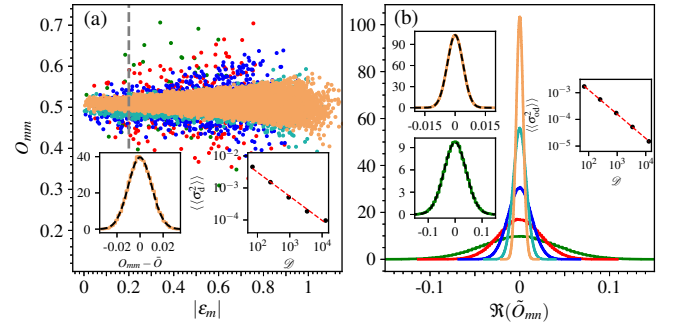


Figure 3. Signature of ETH in the non-Hermitian SYK model. (a) Diagonal elements $|\langle R_m|\hat{O}|R_m\rangle|$ of $\hat{O} = \hat{n}_i$, against $|\epsilon_m|$ for system sizes $N = 8, 10, 12, 14, 16$ (green, red, blue, sea green, orange) and for a single random realization. Similar to Fig. 2, fluctuations here are also suppressed as system size increases. However, unlike the random ensemble case, the spread around the mean is not uniform across the energy range. High-energy states show more deviation than the low-energy ones, which is a characteristic feature of the Hermitian SYK Hamiltonian. Bottom left inset: The histogram of $[O_{mmm} - \bar{O}]$ for eigenstates within the range $|\epsilon_m| \leq 0.2$ (for $N = 16$ and 20 random realizations of the Hamiltonian) is fitted well by a Gaussian curve (black dashed). The bottom right inset depicts linear decay (plotted in logarithmic scale) of variance of diagonal term $\langle\langle\sigma_d^2\rangle\rangle$ with Hilbert space dimension \mathcal{D} for different system sizes and random realizations of the Hamiltonian that are considered exactly the same as in Fig. 2(a). (b) Distribution of the $\Re[\tilde{O}]_{m\neq n}$, obtained for eigenenergies as in (a) (for system sizes $N = 8, 10, 12, 14, 16$, and marked by green, red, blue, sea green, and orange color, respectively). As the Gaussian fits shown for $N = 8$ (top left inset) and 16 (bottom left inset), and the exponential decay of the off-diagonal variance $\langle\langle\sigma_{od}^2\rangle\rangle$ (all the parameters considered for this are same as in Fig. 2(b)) with the Hilbert space dimension \mathcal{D} highlight, by correctly modifying the off-diagonal description the non-Hermitian SYK model displays the signatures of ETH.

the non-Hermitian counterpart of the SYK model [34, 69–72]. The SYK model consists of N fermionic modes with disordered all-to-all interactions, described by (see also [82–84])

$$H_{\text{nh}}^{\text{SYK}_4} = \frac{1}{(2N)^{\frac{3}{2}}} \sum_{i_1 i_2 j_1 j_2} J_{i_1 i_2 : j_1 j_2} c_{i_1}^\dagger c_{i_2}^\dagger c_{j_1} c_{j_2}. \quad (11)$$

Here, we consider the variant with spinless complex fermions, with c_i as defined before. The real and imaginary parts of $J_{i_1 i_2 : j_1 j_2}$ are independent and normally distributed. The non-Hermitian version is obtained by choosing complex $J_{i_1 i_2 : j_1 j_2}$ for the diagonal elements and imposing $J_{i_1 i_2 : j_1 j_2}^* \neq J_{j_1 j_2 : i_1 i_2}$ for the off-diagonals. The following behavior is generic also for other choices of complex interaction amplitudes, see Appendix B for details.

As for the random ensemble, we consider expectation values of the local observable $\hat{O} = \hat{n}_i$, see Fig. 1(c). Again, the diagonal elements for the non-Hermitian SYK model remain in accordance with its Hermitian counterpart and show the characteristics of the ETH. In the bare off-

diagonal terms, strong fluctuations are prominent that can be seen in the zoomed inset. Subtracting the contribution coming solely from the nonorthogonality relation, i.e., employing Eq. (10), we again obtain clearly the signatures of ETH as well as the off-diagonal terms, see Fig. 1(e).

For completeness, in Fig. 3 we reproduce the analysis analogous to Fig. 2. As before, the diagonal elements $|\langle R_m | \hat{O} | R_m \rangle|$ converge to the mean value [Fig. 3(a)]; however, unlike the random ensemble case, the behavior is not uniform in $|\epsilon_m|$, with low-energy states (small $|\epsilon_m|$) converging faster. This behavior is in accordance with the one for the Hermitian case [18]. To strengthen our numerical claim, in the inset (bottom left) we present the histogram of $[\langle R_m | \hat{O} | R_m \rangle - O(\bar{E})]$ for eigenstates within $|\epsilon_m| \leq 0.2$, where \bar{E} is the average energy within the disk, using $N = 16$ and 20 random realizations. The profile accurately coincides with a Gaussian distribution (black dashed). A similar analysis for the off-diagonal terms is shown in Fig. 3(b), where we plot the scaling of the real part of $\tilde{O}_{mn} = O_{mn} - \langle R_m | R_n \rangle \bar{O}$, $m \neq n$ for system sizes $N = 8, 10, 12, 14, 16$. Also, for this data, we find excellent agreement with a Gaussian and exponential suppression of the variance $\langle \langle \sigma_{\text{od}}^2 \rangle \rangle$ with system size.

Discussion.— In this work, we generalized the notion of ETH for non-Hermitian systems. While diagonal elements in the right eigenbasis directly reproduce the ETH features predicted for their Hermitian counterparts, off-diagonal elements can display strong fluctuations, which we found to arise due to the non-orthogonality of non-Hermitian eigenvectors. We introduced a modified ETH prediction that by removing the corresponding trivial but significant contributions becomes analog to the Hermitian ETH formalism. Our numerical analysis confirms the non-Hermitian ETH relation for the random matrix ensemble as well as for a physical model represented by a non-Hermitian SYK Hamiltonian. We hope these findings to stimulate further investigations, in particular to further test our conjecture summarized in Eqs. (8, 9).

Further, as our work shows, the ETH prediction can be faithfully captured only when the local observables are probed using the right (or left) eigenvectors of the model. Such states are those that are naturally prepared through non-Hermitian time evolution, opening the way for direct tests of the framework on experimental platforms. Moreover, we expect these considerations to help clarify the correct choice of basis for other non-Hermitian scenarios and observables as well.

Acknowledgements.— We gratefully acknowledge useful discussions with Philipp Uhrich. We acknowledge support by the ERC Starting Grant StrEnQTh (project ID 804305), MUR FARE project DAVNE, Provincia Autonoma di Trento, and by Q@TN, the joint lab between University of Trento, FBK-Fondazione Bruno Kessler, INFN-National Institute for Nuclear Physics and CNR-National Research Council. The project is funded within

the QuantERA II Programme that has received funding from the European Union's Horizon 2020 research and innovation programme under Grant Agreement No 101017733. This project has received funding by the European Union under Horizon Europe Programme - Grant Agreement 101080086 - NeQST. Views and opinions expressed are however those of the author(s) only and do not necessarily reflect those of the European Union or the European Commission. Neither the European Union nor the granting authority can be held responsible for them. S.B. acknowledges CINECA for the use of HPC resources under ISCRA-C project ISSYK-2 (HP10CP8XXF).

APPENDIX

A. TIME EVOLUTION UNDER NON-HERMITIAN HAMILTONIAN

In this section, we discuss the fate of an initial state when it is evolved under any generic non-Hermitian Hamiltonian H_{nh} , as given in Eq. (4) and also shown in the schematic presented in Fig. 1(a) of the main text. In this regard, it is illustrative to first consider two scenarios that can commonly arise, one that drives the system into a single eigenstate and another one that produces a diagonal ensemble in analogy to Hermitian time evolution, before coming to the general case.

Case I: *Complex ϵ_m 's with a non-degenerate $\max\{s_m\} = s_{\tilde{m}}$.* Separating diagonal and off-diagonal terms in Eq. (4), and introducing the decomposition of the complex energies in real and imaginary parts, $\epsilon_m = w_m + is_m$, with $w_m, s_m \in \mathbb{R}$, we have

$$\rho(t) = \sum_m e^{2ts_m} a_{mm} |R_m\rangle \langle R_m| + \sum_{m \neq n} e^{-it(w_m - w_n)} e^{t(s_m + s_n)} a_{mn} |R_m\rangle \langle R_n|. \quad (12)$$

At large times, $\rho(t)$ eventually converges to the right eigenvector with slowest decay rate [85],

$$\rho(t) \xrightarrow{t \rightarrow \infty} e^{2ts_{\tilde{m}}} a_{\tilde{m}\tilde{m}} |R_{\tilde{m}}\rangle \langle R_{\tilde{m}}|. \quad (13)$$

Suitably normalized, observables will be given by $\langle R_{\tilde{m}} | \hat{O} | R_{\tilde{m}} \rangle$.

Case II: *All ϵ_m 's real (Parity-Time symmetric case).* In this case, Eq. (4) reduces to

$$\rho(t) = \sum_m a_{mm} |R_m\rangle \langle R_m| + \sum_{m \neq n} a_{mn} e^{-it(w_m - w_n)} |R_m\rangle \langle R_n|. \quad (14)$$

As in the Hermitian case assuming irrelevance of resonances at large times, this state evolves into a diagonal ensemble consisting of the right eigenvectors [80, 85],

$$\rho(t) \xrightarrow{t \rightarrow \infty} \sum_m a_{mm} |R_m\rangle \langle R_m|. \quad (15)$$

Also here, observables at long times are determined by (suitably weighted) matrix elements $\langle R_m | \hat{O} | R_n \rangle$.

General Case: *Arbitrary non-Hermitian time evolution.* For an arbitrary non-Hermitian time evolution of any observable \hat{O} , Eq. (4) predicts

$$\begin{aligned} \text{Tr}(\hat{O}\rho(t)) &= \sum_{mn} e^{-it\phi_{mn}} a_{mn} \text{Tr}(\hat{O}|R_m\rangle\langle R_n|), \\ &= \sum_{mn} e^{-it\phi_{mn}} a_{mn} \sum_k \langle R_k | \hat{O} | R_m \rangle \langle R_n | L_k \rangle, \\ &= \sum_{mn} e^{-it\phi_{mn}} a_{mn} \langle R_n | \hat{O} | R_m \rangle. \end{aligned} \quad (16)$$

Here, we have taken the trace in the biorthogonal basis that satisfies the completeness relation $\sum_m |R_m\rangle\langle L_m| = \mathbb{I}$, and used the relation $\langle R_n | L_k \rangle = \delta_{nk}$. Again, observables are evaluated as a (time-evolving) function of matrix elements in the right eigenvectors.

As these considerations illustrate, states determined by the right eigenvectors of the model are naturally prepared. This operational interpretation justifies the preference of the associated basis over the biorthogonal basis when we aim at the computation of physically relevant quantities. Similar justification also holds for the set of left eigenvectors $\{\langle L_m|\}$ of the model, which can be realized when we consider the evolution of an initial state under H_{nh}^\dagger .

B. DETAILS ON NUMERICAL COMPUTATIONS

In this section, we elaborate on the numerical techniques we have employed to obtain the main results of our work. We start our discussion by describing the construction of the random non-Hermitian matrix H_{nh} using the Ginibre ensemble. Subsequently, we detail the construction and diagonalization of the non-Hermitian Sachdev–Ye–Kitaev model. Furthermore, we compare the results for other choices of non-Hermitian SYK Hamiltonians.

I. Non-Hermitian random matrices

Given any non-Hermitian Hamiltonian H_{nh} , we can obtain its set of left and right eigenvectors using the similarity transformation given by

$$H_{\text{nh}} = PDP^{-1} = \sum_m \epsilon_m |R_m\rangle\langle L_m|, \quad (17)$$

where the vectors $|R_m\rangle$ ($\langle L_m|$) construct the columns (rows) of P (P^{-1}) and D is a diagonal matrix with entries $D_{mm} = \epsilon_m$. As a result, we have $\langle L_m | R_n \rangle = \delta_{mn}$. In addition, we choose the normalization $\langle R_m | R_m \rangle = 1$.

For the random ensemble study, we construct the non-Hermitian random matrix H_{nh} by drawing its elements

from the complex Ginibre ensemble. We start with a representation of H_{nh} in the fermionic basis as follows

$$H_{\text{nh}} = \sum_{mn} c_m^\dagger \mathcal{H}_{mn} c_n. \quad (18)$$

We next choose $\mathcal{H}_{mn} = \mathcal{A}_{mn} + i\mathcal{B}_{mn}$, where \mathcal{A}_{mn} and \mathcal{B}_{mn} are chosen independently from a Gaussian distribution with zero mean and variance $\frac{1}{2\mathcal{D}}$. We then use the exact diagonalization technique to bring the Hamiltonian \mathcal{H} in the form as given in Eq. (17).

Using the representation given in Eq. (18), it is also straightforward to define fermionic local observables that draw close analogy to the investigation on the non-Hermitian SYK model. As stated in the main text, for our purposes we choose $\hat{O} = \hat{n}_i = c_i^\dagger c_i$, where due to symmetry the mode i can be chosen arbitrarily.

II. Non-Hermitian Sachdev–Ye–Kitaev model

The interaction amplitudes in the standard Hermitian SYK Hamiltonian of complex fermions H^{SYK_4} are considered as zero mean Gaussian random variables with $\text{var}(\text{Re}[J_{i_1 i_2; j_1 j_2}]) = J^2$, $\text{var}(\text{Imag}[J_{i_1 i_2; j_1 j_2}]) = 0$ if $i_1 = j_1, i_2 = j_2$, and $\text{var}(\text{Re}[J_{i_1 i_2; j_1 j_2}]) = \text{var}(\text{Im}[J_{i_1 i_2; j_1 j_2}]) = J^2/2$, otherwise. Usually, the overall scale J is set to unity.

In case of the non-Hermitian SYK Hamiltonian, we generically choose all the amplitudes to be complex random variables, i.e., $J_{i_1 i_2; j_1 j_2} = \alpha_{i_1 i_2; j_1 j_2} + i\beta_{i_1 i_2; j_1 j_2}$, where $\alpha_{i_1 i_2; j_1 j_2}$ and $\beta_{i_1 i_2; j_1 j_2}$ are independent random numbers chosen from Gaussian distribution with zero mean and variance $1/2$. We additionally consider $J_{i_1 i_2; j_1 j_2}^* \neq J_{j_1 j_2; i_1 i_2}$, for the off-diagonal elements.

Similar to the Hamiltonian matrix construction for the Hermitian SYK model as mentioned in Ref. [34], we construct the non-Hermitian Hamiltonian matrix in the fermionic Fock basis states $|s_a\rangle$ for the half-filled sector, so $a = 1, \dots, \mathcal{D}$. The matrix elements are then computed as $\langle s_a | H_{\text{nh}}^{\text{SYK}_4} | s_b \rangle$, where s_a and s_b represent N -bit strings of equal number of 0 and 1 bits denoting empty and occupied fermionic modes, respectively. For the Hamiltonian in Eq. (11), the non-zero matrix elements correspond to the Hamming distance $d(s_a, s_b) = 0, 2, 4$. We choose these elements as complex random variables with properties mentioned in the previous paragraph. While populating the elements into the Hamiltonian matrix, we ensure the antisymmetry of the interaction amplitudes under the permutation of the subscripts. In this way, a single realization of the non-Hermitian SYK Hamiltonian is constructed. We diagonalize this Hamiltonian in the form of Eq. (17) in order to compute the relevant properties.

For both the Ginibre ensemble and the non-Hermitian SYK Hamiltonian, we evaluate diagonal and off-diagonal matrix elements of observables with respect to the eigenstates of the diagonalized Hamiltonian. In addition, we

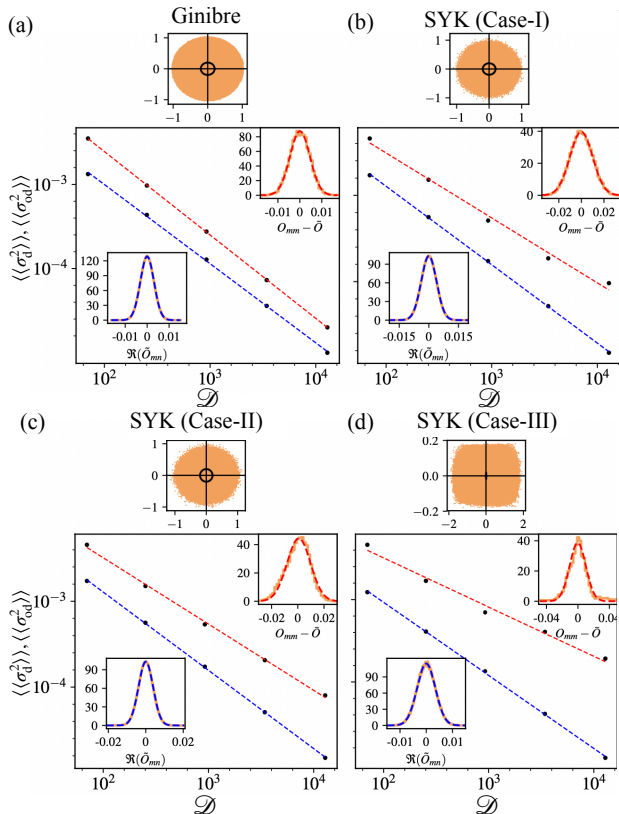


Figure 4. Generic behavior of fluctuations of local operators computed for the eigenbasis of SYK model for different choices of complex interaction elements $J_{i_1 i_2 : j_1 j_2}$. In all the cases, we plot the decay of fluctuations of diagonal ($\langle\langle\sigma_d^2\rangle\rangle$), linearly fitted with dotted red line) and off-diagonal matrix elements ($\langle\langle\sigma_{od}^2\rangle\rangle$), linearly fitted with dotted blue line) with the Hilbert space dimension \mathcal{D} (for $N = 8, 10, 12, 14, 16$) and show the Gaussian fits of the data for $N = 16$ in the insets. Additionally, on top of each plot, we mark the region of the energy subspace from which the eigenstates are sampled. For comparison, we also present the results already shown in the main text: (a) the Ginibre ensemble and (b) the non-Hermitian SYK model Case I. The qualitative feature remain the same for different choices of the complex interaction elements $J_{i_1 i_2 : j_1 j_2}$, (c) SYK Case II with real random diagonal elements but complex random off-diagonal elements satisfying $J_{i_1 i_2 : j_1 j_2}^* \neq J_{j_1 j_2 : i_1 i_2}$; (d) SYK Case III, with complex random diagonal elements and complex random off-diagonal elements with $J_{i_1 i_2 : j_1 j_2}^* = J_{j_1 j_2 : i_1 i_2}$. All the plots clearly show linear decay of fluctuations with \mathcal{D} in the log-log scale. The qualitative agreement of the plots thus shows the generality of the ETH features, independent of the choice of complex couplings.

consider multiple realizations to improve the statistics in our analysis. Since we perform full-diagonalization of the matrices, we employ MPI [86] methods to solve different realizations in parallel, which reduces the computation time significantly.

III. Other choices of Non-Hermitian SYK model

In this subsection, we show that our results generically apply for other choices of non-Hermiticity of the SYK Hamiltonian. All the results presented in the main text are obtained for the choice mentioned in the previous subsection, which we refer to as Case I. However, we can also consider real random diagonal elements, but complex random off-diagonal elements satisfying $J_{i_1 i_2 : j_1 j_2}^* \neq J_{j_1 j_2 : i_1 i_2}$. We call this choice Case II. Furthermore, we can choose the diagonal elements as complex random variables, but with $J_{i_1 i_2 : j_1 j_2}^* = J_{j_1 j_2 : i_1 i_2}$, which we refer to as Case III.

In Fig. 4, we illustrate and compare the key characteristics of the ETH for these different choices of the non-Hermitian SYK Hamiltonian. For comparison, we also reproduce the results of the Ginibre ensemble and SYK Case I in (a) and (b), which have already been presented in the main text. The overlaying complex eigenvalues of multiple realizations are shown at the top of each panel corresponding to the different cases. These also show the region of the eigenstates selected for our analysis. Like in the main text, we obtain exponentially suppressed and Gaussian fluctuations for the diagonal and off-diagonal elements of the observable. The exponential law with respect to system-size is demonstrated by the linear trend of $\langle\langle\sigma_d^2\rangle\rangle$ and $\langle\langle\sigma_{od}^2\rangle\rangle$ with respect to \mathcal{D} in the log-log scales. Therefore, our conclusions do not depend on the microscopic details of the considered non-Hermitian SYK model.

C. ETH FOR EIGENSTATES WITHIN SLICES OF COMPLEX ENERGY SPACE OF RANDOM H_{nh}

In this section, we further substantiate our numerical study done in the main text and shown in Fig. 2. That figure unveils the ETH signature for the random non-Hermitian model constructed using the Ginibre ensemble for the eigenstates lying within the disk of radius $0 \leq |\epsilon_m| \leq 0.2$. Here, we perform a similar analysis but for eigenstates with energies $\epsilon_m = |\epsilon_m|e^{i\Phi}$ such that $0 \leq |\epsilon_m| \leq 1$ and Φ lies within $0.0 \leq |\Phi| \leq 0.05$. In Fig. 5, we plot the behavior for the diagonal terms O_{mm} (panel a) and for the modified off-diagonal terms $[\tilde{O}_{mn}]_{m \neq n}$ (panel b). All the other parameters are the same as considered in Fig. 2. The behavior exactly mimics the one that has been obtained in Fig. 2 and shows the generality of our formalism when applied to eigenstates chosen from any portion of the complex energy spectrum of the model.

D. RESULTS USING BIORTHOGONAL BASIS

In this section, for completeness we present a summary of the results obtained using the biorthogonal basis, for

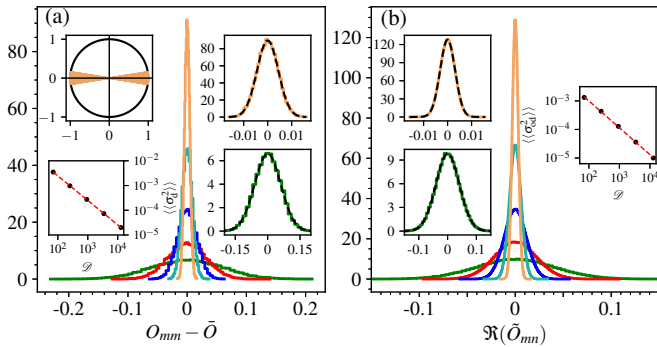


Figure 5. Signature of ETH in a random non-Hermitian Hamiltonian from the Ginibre ensemble. We now consider eigenstates with energy $\epsilon_m = |\epsilon_m|e^{i\Phi}$ lying within slices parametrized by $0 \leq |\epsilon_m| \leq 1$ and $0 \leq |\Phi| \leq 0.05$ of the complex energy spectrum of the model. (a) Histogram of the diagonal terms O_{mm} obtained for system sizes and number of random realizations as in Fig. 2. The right insets show the Gaussian fittings (black dashed) of the histograms for $N = 8$ (bottom, 5000 random realizations) and $N = 16$ (top, 20 random realizations), respectively. Bottom left: the variance of the diagonal data $\langle\langle\sigma_d^2\rangle\rangle$ decays polynomially with Hilbert space dimension \mathcal{D} . (b) Similar analysis for the modified off-diagonal terms $[\tilde{O}_{mn}]_{m \neq n}$. All the behavior obtained here strongly mimics the one obtained in Fig. 2, justifying the generality of our formalism when applied to a set of states chosen from any part of the complex eigenspectrum of the model.

both random matrices H_{nh} using the Ginibre ensemble as well as the non-Hermitian SYK model as described in Eq. (11) of the main text. We consider the same local observable \hat{O} as in the main text. Figure 6 depicts the behavior of $|\langle R_m | \hat{O} | L_n \rangle|$ obtained for a single random realization with $N = 12$. For both models, the behavior of $|\langle R_m | \hat{O} | L_n \rangle|$ remains far from the ETH prediction. In particular, the plots exhibit a “structured” pattern for off-diagonal elements, which signatures off-diagonal and diagonal elements being of the same order. Similar behavior is also reported in Ref. [35].

This behavior is in stark contrast with the elements evaluated in the right (or left) eigenvectors, which, as discussed in the main text, do exhibit behavior compatible with ETH. In contrast to $\langle R_m |$ and $|R_n\rangle$, $\langle R_m |$ and $|L_n\rangle$ are already orthogonal, so a modification to bring predictions into accordance with ETH analogously to Eq. (10) does not seem straightforward.

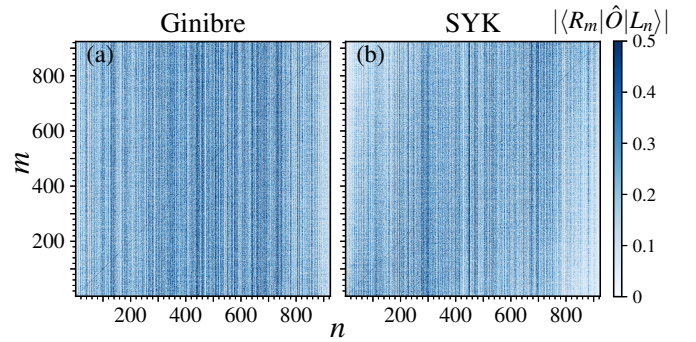


Figure 6. Expectation value of a local operator, computed in the biorthogonal basis of non-Hermitian Hamiltonians for a single random realization. (a) Results for a random matrix H_{nh} obtained from the Ginibre ensemble and (b) for the non-Hermitian SYK model for $N = 12$. In both cases, $|\langle R_m | \hat{O} | L_n \rangle|$ deviates significantly from the ETH prediction as the plots exhibit structured patterns, suggesting strong off-diagonal fluctuations that are comparable to the diagonal elements. This behavior is characteristically different from that obtained for right (or left) eigenvectors of the models, as shown in Fig. 1 in the main text.

[1] J. M. Deutsch, *Quantum statistical mechanics in a closed system*, Phys. Rev. A **43**, 2046 (1991).
 [2] M. Srednicki, *Chaos and quantum thermalization*, Phys. Rev. E **50**, 888 (1994).
 [3] H. Tasaki, *From Quantum Dynamics to the Canonical Distribution: General Picture and a Rigorous Example*, Phys. Rev. Lett. **80**, 1373 (1998).

[4] M. Srednicki, *The approach to thermal equilibrium in quantized chaotic systems*, J. Phys. A: Math. Gen. **32**, 1163 (1999).
 [5] M. Rigol, V. Dunjko, and M. Olshanii, *Thermalization and its mechanism for generic isolated quantum systems*, Nature **452**, 854 (2008).
 [6] L. D’Alessio, Y. Kafri, A. Polkovnikov, and M. Rigol, *From Quantum Chaos and Eigenstate Thermalization to Statistical Mechanics and Thermodynamics*, Adv. Phys. **65**, 239 (2016).
 [7] J. M. Deutsch, *Eigenstate thermalization hypothesis*, Rep. Prog. Phys. **81**, 082001 (2018).
 [8] R. Steinigeweg, J. Herbrych, and P. Prelovšek, *Eigenstate thermalization within isolated spin-chain systems*, Phys. Rev. E **87**, 012118 (2013).
 [9] H. Kim, T. N. Ikeda, and D. A. Huse, *Testing whether all eigenstates obey the eigenstate thermalization hypothesis*, Phys. Rev. E **90**, 052105 (2014).
 [10] W. Beugeling, R. Moessner, and M. Haque, *Finite-size scaling of eigenstate thermalization*, Phys. Rev. E **89**, 042112 (2014).
 [11] R. Nandkishore and D. A. Huse, *Many-Body Localization and Thermalization in Quantum Statistical Mechanics*, Annual Review of Condensed Matter Physics **6**, 15 (2015).
 [12] K. R. Fratus and M. Srednicki, *Eigenstate thermalization in systems with spontaneously broken symmetry*, Phys. Rev. E **92**, 040103(R) (2015).
 [13] V. Alba, *Eigenstate thermalization hypothesis and integrability in quantum spin chains*, Phys. Rev. B **91**, 155123 (2015).
 [14] R. Mondaini, K. R. Fratus, M. Srednicki, and M. Rigol, *Eigenstate thermalization in the two-dimensional transverse field Ising model*, Phys. Rev. E **93**, 032104 (2016).
 [15] T. Mori, *Classical ergodicity and quantum eigenstate thermalization: Analysis in fully connected Ising ferromagnets*, Phys. Rev. E **96**, 012134 (2017).

- [16] B. Neyenhuis, J. Zhang, P. W. Hess, J. Smith, A. C. Lee, P. Richerme, Z.-X. Gong, A. V. Gorshkov, and C. Monroe, *Observation of prethermalization in long-range interacting spin chains*, *Science Advances* **3**, e1700672 (2017).
- [17] P. Basu, D. Das, S. Datta, and S. Pal, *Thermalization of eigenstates in conformal field theories*, *Phys. Rev. E* **96**, 022149 (2017).
- [18] J. Sonner and M. Vielma, *Eigenstate thermalization in the Sachdev-Ye-Kitaev model*, *J. High Energ. Phys.* **2017**, 149 (2017).
- [19] N. Lashkari, A. Dymarsky, and H. Liu, *Eigenstate thermalization hypothesis in conformal field theory*, *J. Stat. Mech.* **033101** (2018).
- [20] C. J. Turner, A. A. Michailidis, D. A. Abanin, M. Serbyn, and Z. Papić, *Quantum many-body scars*, *Nat. Phys.* **14**, 745 (2018).
- [21] D. A. Abanin, E. Altman, I. Bloch, and M. Serbyn, *Colloquium: Many-body localization, thermalization, and entanglement*, *Rev. Mod. Phys.* **91**, 021001 (2019).
- [22] M. Haque and P. A. McClarty, *Eigenstate thermalization scaling in Majorana clusters: From chaotic to integrable Sachdev-Ye-Kitaev models*, *Phys. Rev. B* **100**, 115122 (2019).
- [23] L. Foini and J. Kurchan, *Eigenstate thermalization hypothesis and out of time order correlators*, *Phys. Rev. E* **99**, 042139 (2019).
- [24] A. Dymarsky and K. Pavlenko, *Generalized Eigenstate Thermalization Hypothesis in 2D Conformal Field Theories*, *Phys. Rev. Lett.* **123**, 111602 (2019).
- [25] L. Foini and J. Kurchan, *Eigenstate Thermalization and Rotational Invariance in Ergodic Quantum Systems*, *Phys. Rev. Lett.* **123**, 260601 (2019).
- [26] M. Brenes, T. LeBlond, J. Goold, and M. Rigol, *Eigenstate Thermalization in a Locally Perturbed Integrable System*, *Phys. Rev. Lett.* **125**, 070605 (2020).
- [27] T. Kuwahara and K. Saito, *Eigenstate Thermalization from the Clustering Property of Correlation*, *Phys. Rev. Lett.* **124**, 200604 (2020).
- [28] J. C. Halimeh and P. Hauke, *Origin of staircase prethermalization in lattice gauge theories*, arXiv:2004.07254 [cond-mat.str-el] (2020).
- [29] J. C. Halimeh and P. Hauke, *Staircase Prethermalization and Constrained Dynamics in Lattice Gauge Theories*, arXiv:2004.07248 [cond-mat.quant-gas] (2020).
- [30] C. Murthy, A. Babakhani, F. Igúez, M. Srednicki, and N. Yunger Halpern, *Non-Abelian eigenstate thermalization hypothesis*, arXiv:2206.05310 [quant-ph] (2022).
- [31] J. Wang, M. H. Lamann, J. Richter, R. Steinigeweg, A. Dymarsky, and J. Gemmer, *Eigenstate Thermalization Hypothesis and Its Deviations from Random-Matrix Theory beyond the Thermalization Time*, *Phys. Rev. Lett.* **128**, 180601 (2022).
- [32] S. Sugimoto, R. Hamazaki, and M. Ueda, *Eigenstate Thermalization in Long-Range Interacting Systems*, *Phys. Rev. Lett.* **129**, 030602 (2022).
- [33] Z. Y. Zhou, G. X. Su, J. C. Halimeh, R. Ott, Hui Sun, P. Hauke, B. Yang, Z. S. Yuan, J. Berges, and J. W. Pan, *Thermalization dynamics of a gauge theory on a quantum simulator*, *Science* **377**, 311 (2022).
- [34] S. Bandyopadhyay, P. Urich, A. Paviglianiti, and P. Hauke, *Universal equilibration dynamics of the Sachdev-Ye-Kitaev model*, *Quantum* **7**, 1022 (2023).
- [35] G. Cipolloni and J. Kudler-Flam, *Non-Hermitian Hamiltonians Violate the Eigenstate Thermalization Hypothesis*, arXiv:2303.03448 [cond-mat.stat-mech] (2023).
- [36] C. M. Bender and S. Boettcher, *Real Spectra in Non-Hermitian Hamiltonians Having PT Symmetry*, *Phys. Rev. Lett.* **80**, 5243 (1998).
- [37] B. B. Wei and L. Jin, *Universal Critical Behaviours in Non-Hermitian Phase Transitions*, *Sci Rep* **7**, 7165 (2017).
- [38] R. E. Ganainy, K. G. Makris, M. Khajavikhan, Z. H. Musslimani, S. Rotter, and D. N. Christodoulides, *Non-Hermitian physics and PT symmetry*, *Nat. Phys.* **14**, 11 (2018).
- [39] Ş. K. Özdemir, S. Rotter, F. Nori, and L. Yang, *Parity-time symmetry and exceptional points in photonics*, *Nature Materials* **18** 783 (2019).
- [40] Y. Ashida, Z. Gong, and M. Ueda, *Non-Hermitian Physics*, *Advances in Physics* **69**, 3 (2020).
- [41] A. Biella and M. Schiró, *Many-Body Quantum Zeno Effect and Measurement-Induced Subradiance Transition*, *Quantum* **5**, 528 (2021).
- [42] F. Minganti, A. Miranowicz, R. W. Chhajlany, and F. Nori, *Quantum exceptional points of non-Hermitian Hamiltonians and Liouvillians: The effects of quantum jumps*, *Phys. Rev. A* **100**, 062131 (2019).
- [43] M. A. Miri and A. Alú, *Exceptional points in optics and photonics*, *Science* **363**, eaar7709 (2019).
- [44] H. Zhou, J. Yeon Lee, S. Liu, and B. Zhen, *Exceptional surfaces in PT -symmetric non-Hermitian photonic systems*, *Optica* **6**, 190 (2019).
- [45] R. Franchi, S. Biasi, D. Piciocchi, and L. Pavesi, *The infinity-loop microresonator: A new integrated photonic structure working on an exceptional surface*, *APL Photonics* **8**, 056111 (2023).
- [46] G. Demange and E. Maria Graefe, *Signatures of three coalescing eigenfunctions*, *J. Phys. A: Math. Theor.* **45** 025303 (2012).
- [47] K. Ding, G. Ma, M. Xiao, Z. Q. Zhang, and C. T. Chan, *Emergence, Coalescence, and Topological Properties of Multiple Exceptional Points and Their Experimental Realization*, *Phys. Rev. X* **6**, 021007 (2016).
- [48] S. Yao and Z. Wang, *Edge States and Topological Invariants of Non-Hermitian Systems*, *Phys. Rev. Lett.* **121**, 086803 (2018).
- [49] S. Longhi, *Probing non-Hermitian skin effect and non-Bloch phase transitions*, *Phys. Rev. Research* **1**, 023013 (2019).
- [50] K. Zhang, Z. Yang, and C. Fang, *Correspondence between Winding Numbers and Skin Modes in Non-Hermitian Systems*, *Phys. Rev. Lett.* **125**, 126402 (2020).
- [51] L. Pan, X. Chen, and Y. Chen, *Non-Hermitian linear response theory*, *Nat. Phys.* **16**, 767 (2020).
- [52] K. T. Geier and P. Hauke, *From Non-Hermitian Linear Response to Dynamical Correlations and Fluctuation-Dissipation Relations in Quantum Many-Body Systems*, *PRX Quantum* **3**, 030308 (2022).
- [53] J. Wiersig, *Enhancing the Sensitivity of Frequency and Energy Splitting Detection by Using Exceptional Points: Application to Microcavity Sensors for Single-Particle Detection*, *Phys. Rev. Lett.* **112**, 203901 (2014).
- [54] W. Chen, Ş. K. Özdemir, G. Zhao, J. Wiersig, and L. Yang, *Exceptional points enhance sensing in an optical microcavity*, *Nature* **548**, 192 (2017).
- [55] H. Hodaei, A. U Hassan, S. Wittek, H. G. Gracia, R. E. Ganainy, D. N Christodoulides, M. Khajavikhan, *En-*

- hanced sensitivity at higher-order exceptional points, *Nature* **548**, 187 (2017).
- [56] J. C. Budich and E. J. Bergholtz, *Non-Hermitian Topological Sensors*, *Physical Review Letters* **125**, 180403 (2020).
- [57] A. McDonald and A. A. Clerk, *Exponentially-enhanced quantum sensing with non-Hermitian lattice dynamics*, *Nat Commun* **11**, 5382 (2020).
- [58] G. Di Fresco, B. Spagnolo, D. Valenti, and A. Carollo, *Metrology and multipartite entanglement in measurement-induced phase transition*, arXiv:2302.10132 [quant-ph] (2023).
- [59] Y. Choi, S. Kang, S. Lim, W. Kim, J. Ryul Kim, J. Hyung Lee, and K. An, *Quasieigenstate Coalescence in an Atom-Cavity Quantum Composite* *Phys. Rev. Lett.* **104**, 153601 (2010).
- [60] J. Li, A. K. Harter, J. Liu, L. de Melo, Y. N. Joglekar, and L. Luo, *Observation of parity-time symmetry breaking transitions in a dissipative floquet system of ultracold atoms*, *Nat. Commun.* **10**, 1 (2019).
- [61] W. Cao, X. Lu, X. Meng, J. Sun, H. Shen, and Y. Xiao, *Reservoir-Mediated Quantum Correlations in Non-Hermitian Optical System*, *Phys. Rev. Lett.* **124**, 030401 (2020).
- [62] F. Özlük, T. Lappe, G. Hellmann, J. Schmitt, J. Klaers, F. Vewinger, J. Kroha, and M. Weitz, *Observation of a non-Hermitian phase transition in an optical quantum gas*, *Science*, **372**, 88 (2021).
- [63] M. De Carlo, F. De Leonardis, R. A. Soref, L. Colatorti, and V. M. N. Passaro, *Non-Hermitian Sensing in Photonics and Electronics: A Review*, *Sensors*, **22** (11), 3977 (2022).
- [64] J. Ginibre, *Statistical Ensembles of Complex, Quaternion, and Real Matrices*, *J. Math. Phys.* **6**, 440 (1965).
- [65] R. Hamazaki, K. Kawabata, and M. Ueda, *Non-Hermitian Many-Body Localization*, *Phys. Rev. Lett.* **123**, 090603 (2019).
- [66] G. Akemann, M. Kieburg, A. Mielke, and T. Prosen, *Universal Signature from Integrability to Chaos in Dissipative Open Quantum Systems*, *Phys. Rev. Lett.* **123**, 254101 (2019).
- [67] L. Sá, P. Ribeiro, and T. Prosen, *Complex Spacing Ratios: A Signature of Dissipative Quantum Chaos*, *Phys. Rev. X* **10**, 021019 (2020).
- [68] S. Shivam, A. De Luca, D. A. Huse, and A. Chan, *Many-body quantum chaos and emergence of Ginibre ensemble*, arXiv e-prints arXiv:2207.12390 (2022).
- [69] S. Sachdev and J. Ye, *Gapless spin-fluid ground state in a random quantum Heisenberg magnet*, *Phys. Rev. Lett.* **70**, 3339 (1993).
- [70] S. Sachdev, *Bekenstein–Hawking Entropy and Strange Metals*, *Phys. Rev. X* **5**, 041025 (2015).
- [71] J. Maldacena and D. Stanford, *Remarks on the Sachdev-Ye-Kitaev model*, *Phys. Rev. D* **94**, 106002 (2016).
- [72] Y. Gu, A. Kitaev, S. Sachdev, and G. Tarnopolsky, *Notes on the complex Sachdev-Ye-Kitaev model*, *J. High Energ. Phys.* **2020**, 157 (2020).
- [73] W. Beugeling, R. Moessner, and M. Haque, *Off-diagonal matrix elements of local operators in many-body quantum systems*, *Phys. Rev. E* **91**, 012144 (2015).
- [74] D. J. Luitz and Y. B. Lev, *Anomalous Thermalization in Ergodic Systems*, *Phys. Rev. Lett.* **117**, 170404 (2016).
- [75] T. LeBlond, K. Mallayya, L. Vidmar, and M. Rigol, *Entanglement and matrix elements of observables in interacting integrable systems*, *Phys. Rev. E* **100**, 062134 (2019).
- [76] J. Richter, A. Dymarsky, R. Steinigeweg, and J. Gemmer, *Eigenstate thermalization hypothesis beyond standard indicators: Emergence of random-matrix behavior at small frequencies*, *Phys. Rev. E* **102**, 042127 (2020).
- [77] L. Herviou, N. Regnault, and J. H. Bardarson, *Entanglement spectrum and symmetries in non-Hermitian fermionic non-interacting models*, *SciPost Phys.* **7**, 069 (2019).
- [78] K. Kawabata, K. Shiozaki, and S. Ryu, *Many-body topology of non-Hermitian systems*, *Phys. Rev. B* **105**, 165137 (2022).
- [79] R. Modak and B. Prasad Mandal, *Eigenstate entanglement entropy in a PT-invariant non-Hermitian system*, *Phys. Rev. A* **103**, 062416 (2021).
- [80] A. McDonald, R. Hanai, and A. A. Clerk, *Nonequilibrium stationary states of quantum non-Hermitian lattice models*, *Phys. Rev. B* **105**, 064302 (2022).
- [81] R. Mondaini and M. Rigol, *Eigenstate thermalization in the two-dimensional transverse field Ising model. II. Off-diagonal matrix elements of observables*, *Phys. Rev.* **96**, 012157 (2017).
- [82] P. Zhang, S. Kai Jian, C. Liu, and X. Chen, *Emergent Replica Conformal Symmetry in Non-Hermitian SYK Chains*, *Quantum* **5**, 579 (2021).
- [83] W. Cai, S. Cao, X. Hui Ge, M. Matsumoto, and S. Jin Sin, *Non-Hermitian quantum system generated from two coupled Sachdev-Ye-Kitaev models*, *Phys. Rev. D* **106**, 106010 (2022).
- [84] A. M. García-García, L. Sá, and J. J. M. Verbaarschot, *Symmetry Classification and Universality in Non-Hermitian Many-Body Quantum Chaos by the Sachdev-Ye-Kitaev Model*, *Phys. Rev. X* **12**, 021040 (2022).
- [85] S. Gopalakrishnan and M. J. Gullans, *Entanglement and purification transitions in non-Hermitian quantum mechanics*, *Phys. Rev. Lett.* **126**, 170503 (2021).
- [86] Message Passing Interface Forum. MPI: A Message-Passing Interface Standard Version 4.0, 2021.